Photogrammetrie • Fernerkundung • Geoinformation 1/2009, S. 9–21

On-the-job Range Calibration of Terrestrial Laser Scanners with Piecewise Linear Functions

Gábor Molnár, Norbert Pfeifer, Camillo Ressl, Peter Dorninger & Clemens Nothegger, Vienna, Austria

Keywords: Laser Scanning, TLS, calibration, systematic errors

Summary: Phase-shift terrestrial laser scanners, as all other measuring devices, are affected by measurement errors, i.e. errors in range and vertical and horizontal angle. These errors are composed of a random and a systematic part. The systematic errors of the range measurement are in the order of a few millimeters, whereas random range measurement errors are higher.

An on-the-job range calibration method is presented and applied on a real dataset. The method relies on scanned datasets of planar surfaces, so called "patches". Assuming that the measured points are on these patches, parameters of the range correction function, scanner and patch parameters are estimated simultaneously using least squares adjustment.

A continuous piecewise linear correction function is suggested, and its parameters are estimated using the proposed adjustment method. This is, from the theoretical point of view, the main contribution of this paper. It effectively exploits the massive overdetermination provided by terrestrial laser scanning and advances previously suggested self-calibration approaches (Gielsdorf et al. 2004, Bae & Lichti 2007). The actual range correction function for a FARO LS 880HE instrument clearly shows the periodic range errors reported by other authors. The correction function also shows shorter periodic errors not reported before as well as non-periodic systematic errors.

Zusammenfassung: *On-the-Job Entfernungskalibrierung von terrestrischen Laserscannern mit stückweise glatten Funktionen.* Die Winkel- und Streckenmessungen von terrestrischen Laserscannern sind durch zufällige und systematische Fehler verfälscht. Bei der Entfernungsmessung nach dem Phasenvergleichsverfahren sind die systematischen Fehler typischerweise zwar kleiner als die zufälligen Fehler, aber auch schwieriger zu bestimmen. In diesem Artikel wird eine „on the job" Kalibrierungsmethode für die Streckenmessungen präsentiert und an einem realen Datensatz getestet. Die Methode setzt voraus, dass ebene Flächenstücke in der gescannten Punktwolke vorhanden sind. In der Folge werden in einer Ausgleichung nach vermittelnden Beobachtungen die Orientierungsparameter der einzelnen Scanpositionen, die Ebenenparameter und die Parameter für die Entfernungskorrektur simultan berechnet. Letztere ist durch eine stetige, stückweise lineare Korrekturfunktion realisiert. Diese Form der Korrekturfunktion und die simultane Berechnung ihrer Parameter ist der Hauptbeitrag dieses Artikels. Der Ansatz nutzt die in Laserdaten vorhandene Überbestimmung sehr effizient aus und erweitert existierende Selbstkalibrierungsvorschläge (Gielsdorf et al. 2004, Bae & Lichti 2007). Im Beispieldatensatz eines FARO LS 880HE Laserscanners zeigten sich deutliche periodische Korrekturanteile über die auch andere Autoren bereits berichtet haben. Mit der vorgestellten Methode wurden aber auch markante periodische Korrekturanteile mit kürzerer Wellenlänge aufgedeckt – über diese wurde bisher noch nicht berichtet. Zusätzlich wurden auch nicht-periodische Anteile festgestellt.

1 Introduction

Precise and detailed, three-dimensional geometric models are used for multiple purposes such as industrial site reconstruction, heritage documentation, and natural surface monitoring for risk and hazard assessment. Point clouds acquired by a terrestrial laser scanner

DOI: 10.1127/0935-1221/2009/0002 0935-1221/09/0002 $ 3.25

(TLS) are commonly used for automated model generation, as TLS allow for fast and area-wide acquisitions of huge scenes. The continuously increasing performance (i. e. data sampling rates) of such scanners increases also the expectations of the data end-users with respect to accuracy and richness in detail. However, these expectations can often not be fulfilled due to shortcomings of the systems.

TLS based on phase-shift measurement (RÜEGER 1990) have a field of application between less than one meter and up to 100 meter. Commercial systems apply amplitude modulation of the continuously emitted wave (AM-CW). The achievable accuracy of the raw measurements is about 3 millimeters for distances of up to 10 m. However, it has been shown, for example, by LICHTI (2007), AMIRI PARIAN & GRUEN (2005), and SCHNEIDER & MAAS (2007), that the error budget of TLS can be divided into random (precision) and systematic measurement errors following the definition of (MIKHAIL 1976). Hence, both categories of errors may be dealt with individually. For example, random measurement errors as reported by (INGENSAND et al. 2003) can be reduced significantly by suitable averaging techniques (NOTHEGGER & DORNINGER 2009) especially when taking advantage of the high measurement rates of phase-shift scanners (> 100 kHz).

Systematic measurement errors cannot be removed by simple averaging. These errors are often correlated with the measured distance, hence, modifying the average of the measured distances. Thus these errors limit the applicability of terrestrial laser scanning especially if high accuracy, e. g., ± 1 mm, is required. However, systematic measurement errors can be eliminated, or at least reduced, by proper laboratory calibration. However, very often the scanned data still shows remaining systematic errors. Therefore correction methods are required, which can be applied "on-site", termed *on-the-job calibration* or *self calibration.*

In this paper, we propose a method for on-the-job *range* calibration of TLS. It requires multiple scans from identical, planar patches. It can be applied on data acquired on the job, i. e., real project data. Hence, changes of the calibration over time can be dealt with properly. Because of the huge amount of data, such methods are only feasible if they run automatically. The method is based on an overall adjustment of the residuals of the measurements with respect to the planar patches. Simultaneously, the plane parameters of all patches and the registration parameters of the individual scans are determined. The paper starts with an overview on the state-of-the-art in TLS calibration approaches in Section 2. Theory and methods are described in Section 3. In Section 4, we describe the acquisition and the preprocessing of the datasets used for the experiments. The results of the method's application on point clouds, acquired in historic rooms are presented in Section 5 and discussed afterwards.

2 State-of-the-Art

To understand the nature of the systematic errors discussed in this paper, a closer look on the measurement principles of the instruments used is necessary. Systematic errors of the early phase-shift electronic distance measurement devices are summarized by (RÜEGER 1990). He identified additive constant error, scale-error, short-periodic errors and non-linear distance dependent errors. The additive constant error is a constant difference of the true and the measured distance. This is due to the optical and electronic structure of the instrument (the uncompensated optical path length and time delay in the electronics). The scale error is due to the frequency error of the modulating waves. The short-periodic errors are periodic functions of the measured range. The wavelengths of these periodic functions are usually integer divisors of the modulating wavelengths. This can be caused by the optical and/or electrical crosstalk (RÜEGER 1990). Non-linear distance dependent errors are all other distance-dependent errors, which are repeatable and reproducible, but do not fit into the above three classes. These errors are usually modeled with polynomial expressions.

A similar error model was presented by (LICHTI 2007) for phase-shift scanners. The error functions for range measurement correction were the additional constant, scale factor and periodic functions with only the half of

the wavelength of shortest and middle modulating waves. In addition, the dependency of the measured distance from the vertical and horizontal angle of measurement direction was also considered. The actual values of the coefficients of the error functions (additional parameters, APs) were estimated using an adjustment method comparing laser scanner and tachymeter measurements of a set of retro-reflecting targets.

(Ingensand et al. 2003) reported laser scanner range measurements compared with interferometer distances. As the measurements were made with one-meter interval for $0-52$ meters, the short-periodic errors (shorter than 2 meters wavelength) were not seen in the calibration function. They also found an unexpected short-periodic error with a wavelength of approximately 3.4 meters and with increasing amplitude from 3 mm to 27 mm in the distance range from 28 to 52 meters. This indicates that short-periodic errors cannot be regarded as a periodic function with constant amplitude over the entire measurement range.

(Kersten et al. 2008) used spherical objects and reflective targets to evaluate and determine the long-distance measurement errors of new generation laser scanners. They also determined the non-periodic systematic errors for two phase-shift scanners.

The method of range measurement error determination – applied by the authors mentioned above – has significant deficiencies: Because the random error of the range measurements is larger than the systematic errors, the number of the calibration measurements (number of the measured targets) should exceed substantially the number of the calibration function coefficients (additional parameters). This is a very time consuming work, because the scanner measurements should be repeated many times for proper averaging of scanner data, and reference measurements (with tachymeter or interferometer) should be made with short distance intervals to find all possible short-periodic error components over the entire measurement range.

An analysis of short-periodic errors was made by (Dorninger et al. 2008). They defined local plane surface segments (patches) in the dataset of a scanned room, and calculated the distances of individually measured points from the adjusted planar patches. They used patches with an extent in range direction that is slightly longer than the wavelength of the expected systematic error. This method has limitations: the coefficients of periodic errors with longer wavelength than the extent of the patch cannot be determined. But increasing the extent of the patches is also limited, because then also the planarity of the patches on real surfaces decreases.

In an earlier work, a plane-based on-the-job calibration method was suggested by (Gielsdorf et al. 2004). The basic idea is that points measured from different scanner positions and corrected with the proper calibration function should fit on planar patches. The parameters of the calibration function, the exterior orientation of the scanners, and the plane parameters of the patches are estimated using an adjustment process, similarly to a photogrammetric bundle adjustment. (Gielsdorf et al. 2004) applied the method for correcting horizontal and vertical angles. For the ranges they estimated the additive constant error and the scale-error. (Bae & Lichti 2007) applied this method for the FARO LS 880HE laser scanner data, and they estimated for range correction only the additive constant parameter (besides angular correction functions).

The measured distance also depends on the propagation conditions in the atmosphere (not significant on distances up to 50 meters) and on the interaction of the reflecting surface and the laser beam. This second effect ("material-related variance") was examined by (Ingensand et al. 2003). It is often modeled as a function of measured intensity and applied in the laser scanner software.

3 Theory and Method

We assume the following to be given: (i) several scans of the same scene obtained from different scan positions, and (ii) planar features included in the scene.

The method for detecting such planar features (termed *patches* in the following) is not scope of this paper. However, Section 4 on the example data gives a short description of the method we applied.

3.1 *Observations*

Exported *x*, *y*, *z* point coordinates should be converted to spherical coordinates, as the instrument actually measures these values. The spherical coordinates[1] of the i^{th} measured point in the j^{th} scanner space are range, ρ_{ij}, horizontal direction, λ_{ij}, and elevation (vertical) angle, φ_{ij}, which are parameterized in terms of scanner space Cartesian co-ordinates (x_{ij}, y_{ij}, z_{ij}) as follows:

$$\lambda_{ij} = \arctan\left(\frac{y_{ij}}{x_{ij}}\right), \quad \varphi_{ij} = \left(\frac{z_{ij}}{\sqrt{x_{ij}^2 + y_{ij}^2}}\right) \qquad (1.a, b)$$

$$\rho_{ij} = \sqrt{x_{ij}^2 + y_{ij}^2 + z_{ij}^2} + \Delta\rho\,(\mathbf{x}^{\mathbf{AP}}) \qquad (1.c)$$

As a consequence of the aim – correction of range measurements – a range correction function $\Delta\rho$ is introduced in Eq. (1.c). The actual form of the function $\Delta\rho$ will be discussed later. The parameters $\mathbf{x}^{\mathbf{AP}}$ of this correction function are either called "interior orientation parameters", "additional parameters" (AP), in (Lichti 2007), or "calibration parameters" in (Gielsdorf et al. 2004).

3.2 *Functional Model*

In the proposed algorithm, identical planes are observed from different scanner positions, so the range correction function, the scanner orientation parameters and the patch parameters are adjusted simultaneously, with the condition that the measured points are on the patch.

The Cartesian coordinates of the observed range and angle measurements can be calculated using the inverse of Eqs. 1.a – 1.c.

$$\rho_{ij}, \lambda_{ij}, \varphi_{ij}, \rightarrow x_{ij}, y_{ij}, z_{ij} \qquad (2)$$

The Cartesian coordinates of this observed point are denoted as $\boldsymbol{\rho}_{ij}$. To convert these "scanner-based" coordinates to our global (project) coordinate system, the rotation matrix, $\mathbf{M}_j$, and translation vector, $\mathbf{t}_j$ for the j^{th} scanner position are used. The point $\boldsymbol{\rho}'_{ij}$ in the global coordinate system is given by

$$\boldsymbol{\rho}'_{ij} = \mathbf{M}_j \cdot \boldsymbol{\rho}_{ij} + \mathbf{t}_j \qquad (3)$$

The rotation matrix is constructed using the rotation angles around the three axes of the global coordinate system. (Gielsdorf et al. 2004) used quaternion representation for the rotations, but if the initial values of these angles are close to the solution, classical rotation matrix representation is sufficient. The parameters responsible for scanner position and angular attitude are the exterior orientation. Therefore, the rotation angles and translation vector components are denoted as $\mathbf{x}_j^{\mathbf{EO}}$.

The parameters of the k^{th} patch in the global coordinate system are the plane normal $\mathbf{n}_k$ (with $\mathbf{n}^T \cdot \mathbf{n} = 1$) and the patch constant d_k. The patch parameters are combined and denoted as $\mathbf{x}_k^{\mathbf{PP}}$. The orthogonal distance of the measured point $\boldsymbol{\rho}'_{ij}$ from its corresponding patch is:

$$v_{ijk} = \boldsymbol{\rho}'^{T}_{ij} \cdot \mathbf{n}_k - d_k \qquad (4)$$

3.3 *Stochastic Model*

Our aim is to determine the additional parameters, the exterior orientation and the patch parameters such that all points $\boldsymbol{\rho}_{ij}$ lie as close as possible to their respective patch. For doing this simultaneously we apply a least squares adjustment based on Eq. (4). Since $\boldsymbol{\rho}'_{ij}$ in (4) is a function of the original polar measurements (ρ, λ, φ), such a least squares adjustment would require a Gauss-Helmert model minimizing the residuals of these original measurements. Then (4) could be used as constraints with $v_{ijk} \equiv 0$. However, at the present state of our research, we apply a simplified version and use $\boldsymbol{\rho}'_{ij}$ as fixed, but consider Eq. (4) as observation equation (also termed condition); i. e.

$$0 + v_{ijk} = \boldsymbol{\rho}'^{T}_{ij} \cdot \mathbf{n}_k - d_k \qquad (5)$$

Thus, the observation value is zero (i. e. the orthogonal distance of $\boldsymbol{\rho}'_{ij}$ to its patch) and v_{ijk} is the residual. This way we work with a

1 Often phase based TLS work like a "profiler": the emitted laser beam direction rotates in a vertical plane, so the vertical angle, φ_{ij}, is from −90° (nadir) to 270°. This "profiler" makes a half rotation during the measurement process, so the direction angle, λ_{ij}, is between 0° and 180°.

Gauss-Markov model and according to the least squares principle, we need to minimize the sum of squared residuals:

$$\sum_{i,j,k} v_{ijk}^2 = \min \tag{6}$$

However, each point is observed at different distances and at different incidence angles w.r.t. the patches. Therefore the distribution of the orthogonal distance to the respective patch will be different in each $\boldsymbol{\rho}'_{ij}$. Consequently we introduce individual *a priori* weights, p_{ijk} and minimize the weighted sum of squared residuals:

$$\sum_{ijk} p_{ijk} \cdot v_{ijk}^2 = \min \tag{7}$$

The individual weight p (omitting $_{ijk}$) is given by $p = 1/\sigma_n^2$, where σ_n is derived by applying the law of error propagation onto (4). Geometrically σ_n can be interpreted as half of the extension of the error ellipsoid of the point $\boldsymbol{\rho}'_{ij}$ in the direction of the plane normal $\mathbf{n}_k$. This error ellipsoid results from the propagation of the errors in (ρ, λ, φ) into the point $\boldsymbol{\rho}'_{ij}$.

The remainder of this Subsection shows how σ_n can be derived geometrically. The stochastic model can be established by defining standard deviations σ_ρ, σ_λ and σ_φ for original observations (KRAUS 1997). These values are taken from the instrument specification. To calculate the error ellipses of a measured point, a local point-based coordinate system $(\bar{x}\,\bar{y}\,\bar{z})$ is defined (BAE et al. 2005), where this error ellipsoid is in canonical position: its axes are parallel to the axes of the local coordinate system. The $\bar{x}$–axis of this coordinate system is in the range measurement direction; the $\bar{y}$–axis is orthogonal to the $\bar{x}$–axis and orthogonal to the scanner vertical axis. The $\bar{z}$-axis is orthogonal to both, and the three axes follow the right-hand rule. In this local Cartesian coordinate system, the semi-axes of the error ellipsoid are:

$$\sigma_{\bar{x}} = \sigma_{\bar{\rho}}, \quad \sigma_{\bar{y}} = \cos\varphi \cdot \rho \cdot \sigma_\lambda, \quad \sigma_{\bar{z}} = \rho \cdot \sigma_\varphi \tag{8}$$

As $\sigma_{\bar{y}}$ and $\sigma_{\bar{z}}$ increases with the range, the shape of error ellipsoid differs from point to point. The σ_n is half of the extension of the ellipsoid in the plane normal direction. For points with longer measured range, $\sigma_{\bar{y}}$ and $\sigma_{\bar{z}}$ might significantly exceed $\sigma_{\bar{x}}$. To calculate σ_n, the plane normal is transformed into the system $(\bar{x}\,\bar{y}\,\bar{z})$.

On the ellipsoid the point $\mathbf{r} = (\bar{x}_r\,\bar{y}_r\,\bar{z}_r)$ is the tangent point of a plane parallel to the patch (see Fig. 1). The distance of the origin of the coordinate system to this tangent plane equals σ_n. It can be computed in the following way. The normal vector $\mathbf{n}$ of the patch and the ellipsoid gradient in $\mathbf{r}$ must be parallel: $\mathbf{n} \parallel \mathrm{grad}_{ell}(\mathbf{r})$; thus:

$$(n_{\bar{x}};\, n_{\bar{y}};\, n_{\bar{z}}) \parallel \left(\frac{2\,\bar{x}_r}{\sigma_{\bar{x}}^2};\, \frac{2\,\bar{y}_r}{\sigma_{\bar{y}}^2};\, \frac{2\,\bar{z}_r}{\sigma_{\bar{z}}^2}\right) \tag{9}$$

This yields:

$$(\bar{x}_r;\, \bar{y}_r;\, \bar{z}_r) = \frac{s}{2}\left(n_{\bar{x}}\sigma_{\bar{x}}^2;\, n_{\bar{y}}\sigma_{\bar{y}}^2;\, n_{\bar{z}}\sigma_{\bar{z}}^2\right) \tag{10}$$

The scale factor s is computed using the ellipsoid equation:

$$\frac{1}{s^2} = \frac{n_{\bar{x}}^2 \cdot \sigma_{\bar{x}}^2}{4} + \frac{n_{\bar{y}}^2 \cdot \sigma_{\bar{y}}^2}{4} + \frac{n_{\bar{z}}^2 \cdot \sigma_{\bar{z}}^2}{4} \tag{11}$$

Substituting s into Eq. (10) returns $\mathbf{r}$, which finally gives the *a priori* standard deviation of the measurement:

$$\sigma_n = \mathbf{n}^T \cdot \mathbf{r} \tag{12}$$

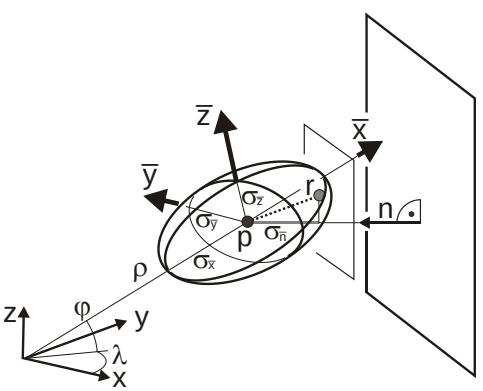

Fig. 1: Error ellipsoid in the measurement based local coordinate system. The σ_n value is half of the extension of error ellipsoid in the direction of the plane normal vector.

Since σ_n depends on the unknown normal vector $\mathbf{n}$, σ_n needs to be recomputed before each iteration step.

3.4 *Formulation of the Adjustment*

By combining all v_{ijk} to a vector $\mathbf{v}$ and generating a diagonal matrix $\mathbf{P}_{ll}$ from all weights p_{ijk}, our minimizing criterion is therefore given by

$$\mathbf{v}^T \mathbf{P}_{ll} \mathbf{v} = \min \tag{13}$$

From Eq. (5) we get after linearization:

$$\mathbf{v} = \mathbf{A}\mathbf{x} - \mathbf{l} \tag{14}$$

where $\mathbf{x}$ is the vector of corrections to the unknown parameters

$$\mathbf{x} = (\mathbf{x}^{\mathbf{AP}}, \mathbf{x}_1^{\mathbf{EO}}, \ldots, \mathbf{x}_J^{\mathbf{EO}}, \mathbf{x}_1^{\mathbf{PP}}, \ldots, \mathbf{x}_K^{\mathbf{PP}}) \tag{15}$$

with J scan positions and K planar patches. $\mathbf{A}$ is the Jacobian of Eq. (5) with respect to $\mathbf{x}$ and $\mathbf{l}$ is the misclosure vector. Constraints need to be defined as the length of each patch normal vector is 1:

$$\sqrt{\mathbf{n}_k^T \cdot \mathbf{n}_k} - 1 = 0 \tag{16}$$

These constrains after linearization can be rewritten in the form:

$$\mathbf{C}\mathbf{x} - \mathbf{w} = 0 \tag{17}$$

where $\mathbf{C}$ is the Jacobian of the constraints with respect to the set of parameters and $\mathbf{w}$ is the misclosure vector. This way we get a Gauss-Markov model with constraints. The respective system of equations can be solved using Lagrange multipliers $\boldsymbol{\mu}$.

$$\begin{bmatrix} \mathbf{A}^T \mathbf{P}_{ll} \mathbf{A} & \mathbf{C}^T \\ \mathbf{C} & \mathbf{0} \end{bmatrix} \cdot \begin{bmatrix} \hat{\mathbf{x}} \\ \boldsymbol{\mu} \end{bmatrix} = \begin{bmatrix} \mathbf{A}^T \mathbf{P}_{ll} \mathbf{l} \\ \mathbf{w} \end{bmatrix} \tag{18}$$

Since the initial values of the parameters are already close to the final solution, one iteration is usually sufficient.

3.5 *Range Correction Function*

The applied range correction function should be mathematically as simple as possible, but also as effective as possible.

Harmonic functions (sine and cosine) with wavelengths reported by other authors seem to be a good choice. This definitely works for short-periodic wavelengths, but it also tries to approach the non-periodic error with periodic functions, which might introduce serious errors. Another disadvantage of harmonic functions is that the correction function does not necessarily have equal amplitude along the whole measurement range. Polynomial functions are also good for non-periodic components, but for realizing short-periodic components higher order terms are required, whose behavior is not very predictable. More complicated error functions could be composed by combining harmonic and polynomial functions.

Because of the mentioned drawbacks of harmonic and polynomial functions we select a piecewise linear range correction function. The measurement range is divided into M equal range intervals. The mathematical form is:

$$\Delta\rho(\rho) = a_i + \frac{a_{i+1} - a_i}{\rho_{i+1} - \rho_i} \cdot (\rho - \rho_i)$$

$$\text{if: } \rho_i \le \rho < \rho_{i+1} \quad \text{with } i = 1, \ldots, M+1 \tag{19}$$

The a_i coefficients are the parameters of the function. The length of the intervals $\delta\rho = \rho_{i+1} - \rho_i$ can be set arbitrarily to some extent. As a lower limit for the interval length, there should be enough measurement points in all intervals of the range, to reduce the effects caused by random errors. An upper limit of $\delta\rho$ is given by the Nyquist-Shannon theorem: $\delta\rho$ must be smaller than half of the shortest wavelength of the short-periodic errors. The shortest wavelength observed by (Dorninger et al. 2008) is the 15 cm wavelength, so the interval length should be shorter than 7.5 cm, and therefore $\delta\rho$ = 5 cm proved to be a good compromise.

Depending on the minimum and maximum range (i. e. the span of ranges) this correction function is applied on, the number of unknown parameters a_i can be quite high and their esti-

mates after the adjustment will be correlated. This property makes this correction function not the best candidate for a *laboratory* calibration, which later is to be applied at different projects with different spans of ranges. It is, however, suitable for *on-the-job* calibration, which is the topic of this paper. There the derived correction function is only applied to the data set, which contains the patches that were used for determining the parameters a_i. In order to get reasonable estimates for all a_i within the span of ranges on site, all range intervals must be covered with range-wise overlapping patches. Therefore a suitable number of planar regions is required on site. Such conditions can be fulfilled for example at manmade sites. If certain range intervals are not covered by at least one patch, then these intervals can not be corrected.

The correction function (19) is of a very general form. The additive constant and the scale error are included implicitly. The latter would lead to a singularity in the adjustment. Consequently proper means for fixing this singularity must be introduced; e. g., known distances between the intersection points of triples of patch planes. Alternatively, one a_i can be fixed. This, however, introduces an artificial scale which appears as a linear trend in the correction function.

4 Data

4.1 *Dataset*

With a FARO LS 880HE scanner, several rooms of Schönbrunn Palace (Vienna, Austria) were scanned during a measurement campaign in May 2007. One of the rooms with approximately 7.4 m by 5.8 m horizontal extension, and with a vaulted ceiling (up to 4 m) was scanned from three scanner positions. The walls of the room are covered with paintings (frescoes in the vaults and on linen, fixed on wooden frames on the walls). The floor is varnished parquet. Fig. 2, left, shows a textured, virtual model of this room. A map of the room indicating the three scanner positions (SP1, SP2, and SP3) is shown in Fig. 2, right. The three point clouds, acquired at the three scanning positions, originally consist of about 40 million points, each. The mean point density at 5 meter distance is about 3 mm.

4.2 *Preprocessing of Data*

The instrument already is equipped with a set of three internal range correction functions: a periodic correction with a wavelength of 60 cm, a polygonal correction function based on range and described as a look-up table, and another look-up table based correction correlated with the intensity of the reflected signal. Individual investigations of these three corrections have shown that the intensity calibration is sufficient, while the other two corrections may not able to cope with the occurring systematic errors properly. Indeed, the influence of the periodic error with a wavelength of 60 cm was reduced but not eliminated sufficiently and periodic errors with different wavelengths are still detectable. Moreover, the polygonal distance correction eliminates the systematic errors only partially (Dorninger et al. 2008). Hence, the internal periodic and the polygonal correction were deactivated, prior to our investigations.

Fig. 2: A textured model of the Bergl-room (left) and a map including the scanner positions (right).

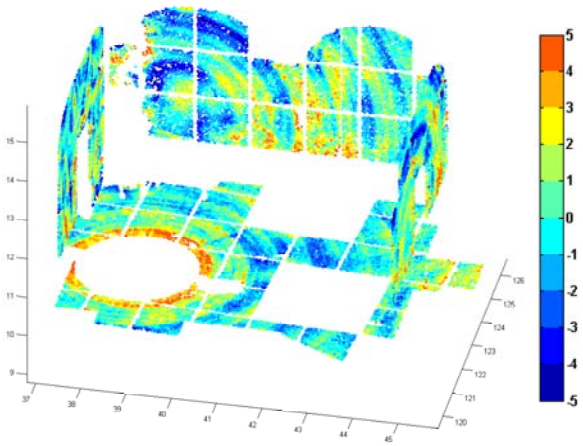

Fig. 3: The dataset of a room captured with FARO LS 880HE instrument. Point colors indicate the distance (in mm) of the measurement points (of SP 2 in Fig. 2) from adjusted planar patches. Circular patterns on the floor and on the walls originate from short-period measurement errors.

For reducing the measurement noise while simultaneously reducing the number of points to be processed, a three-dimensional filtering and thinning approach (NOTHEGGER & DORNINGER 2009) was applied. This allowed reducing the number of points by a factor of 20, resulting in approximately 2 million points per scan.

The first registration of the scans was based on a network of spherical targets, detectable in all point clouds. The reference positions of the targets were determined by tachymetric measurements. The accuracy of this registration is about ± 0.5 cm.

For the on-the-job calibration approach described in the following, planar features ("patches"), identifiable in multiple scans, are necessary. These patches are determined automatically by a two step procedure. First, an automatic segmentation (DORNINGER & NOTHEGGER 2007) is performed, resulting in an assignment of the given points to huge segments representing the walls and the floor. Second, the patches are determined by partitioning the huge segments into subsegments. These are defined in a regular pattern of the local 2D coordinate system of each huge segment. Therefore and because of the known orientation of the scans the patches are identified in all scans.

The patch definition allows for the determination of rectangular patches considering an overlap (in percent), a minimum number of points belonging to a patch, and an *a priori* threshold for outlier elimination. For our experiments, we determined 1 by 1 meter patches, with 10 cm gaps between patches. For outlier elimination we defined a threshold of 1 cm. As the measurements were made in a room, where the strict planarity of the walls and the floor could not be guaranteed, a smaller threshold to eliminate non-planar patches would be favorable. On the other hand, it could not be determined beforehand if the observed deformation of a patch originates from the non-planarity of the feature, or from the systematic range measurement error of the instrument.

According to these parameters, we determined 73 patches. Initially, the plane parameters (**n** and d) for all patches are calculated by independent adjustments. The orthogonal distances of the patch defining points with respect to the planes are shown color coded in Fig. 3 for one scan.

5 Results

Fig. 4 shows the resulting range correction function. Fig. 5 shows the power spectrum of the range correction function. As expected, periodic components with wavelengths of 60 cm and 30 cm can be found in the correc-

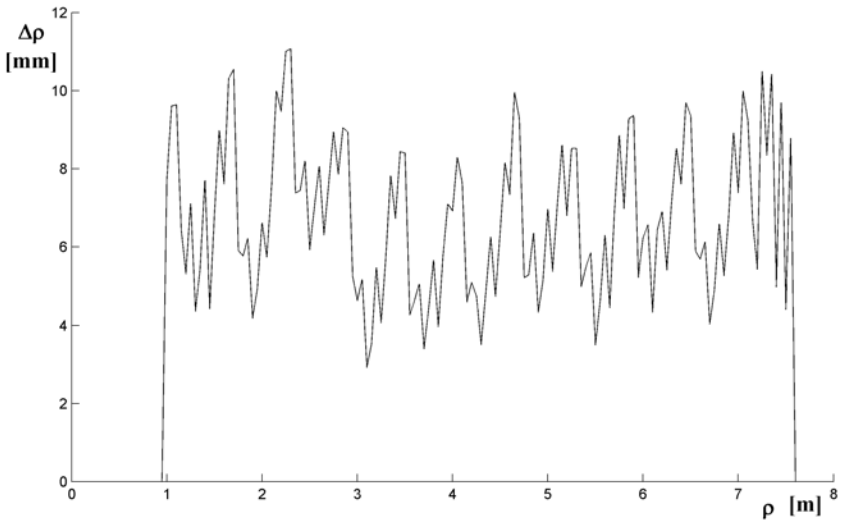

Fig. 4: Range correction function with interval length $\delta\rho$ = 5 cm. Short-periodic systematic errors are clearly visible. The additional constant error of 6.72 mm on average is due to deactivating the internal periodic and polygonal correction.

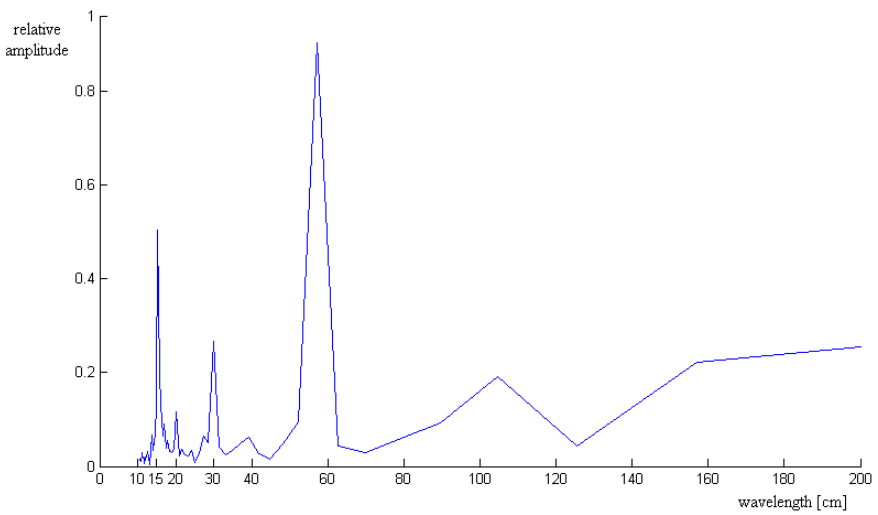

Fig. 5: Power spectrum of the Fast Fourier Transformation of the range correction function. The 60 cm wavelength is dominant, but also 15, 30 and 20 cm show very clear and sharp peaks. No such sharp edges can be identified for longer wavelength components.

tion function, but also higher frequency components (20 and 15 cm) are clearly visible.

Because no external reference distance was given, the scale ambiguity mentioned in Section 3.5 was solved by fixing one a_i. The linear trend induced thereby in the correction function was estimated after the adjustment and removed from the correction function shown in Fig. 4.

In order to show the positive effect of the derived correction function Fig. 6.a and b show the distance of all measured points without and with range correction from the patches. The standard deviation of these distances was 1.62 mm without range correction function (cf. Fig. 6a). In this adjustment process, only the scanner parameters and the patch parameters were estimated. By estimating the range correction function parameters in the adjustment process, the standard deviation of these distances decreased to 1.21 mm. The comparison of Fig. 6.a with b and the decrease in the standard deviation show that the data quality is significantly improved. Outliers were not removed from the dataset (cf. Section 3.2).

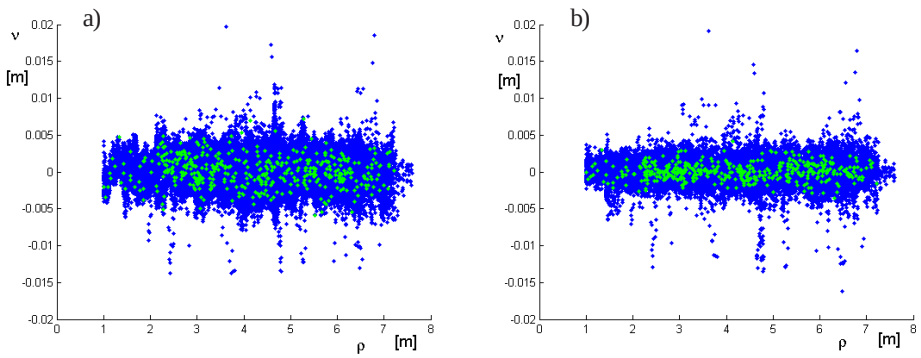

Fig. 6: (a) Distance of originally measured points from the adjusting patches. Blue dots: orthogonal distance (v_{ijk}). Green dots: average of blue dots (bin size 1 cm in range direction). (b) Distance of range-corrected points from the adjusting patches.

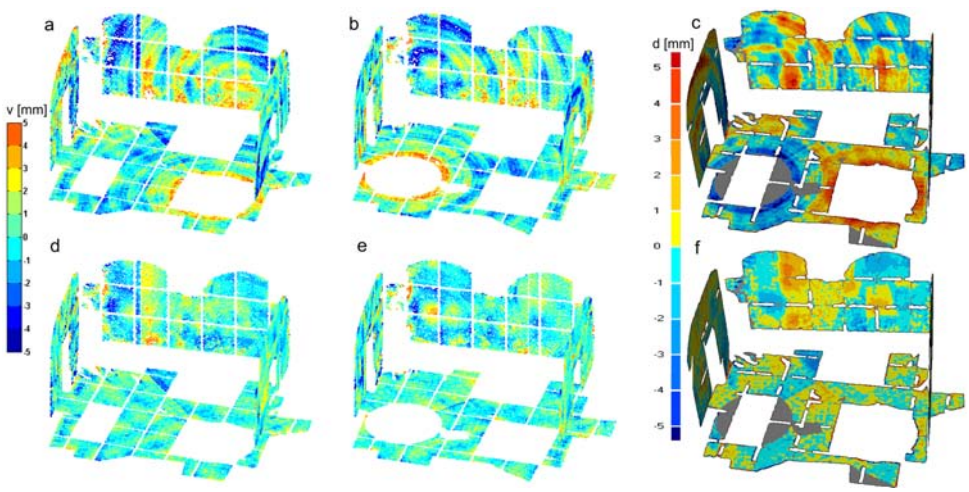

Fig. 7: Distance of measured points from adjusting patches. (a) Scanner position 1 without correction, (b) Scanner position 2 without correction, (c) difference of both scans without correction; (d) Scanner position 1 with correction, (e) Scanner position 2 with correction and (f) difference of both scans with correction. Note: For subfigures (c) and (f) the data of scanner position 1 was triangulated and the distance of the data points of scanner position 2 to this surface is visualized.

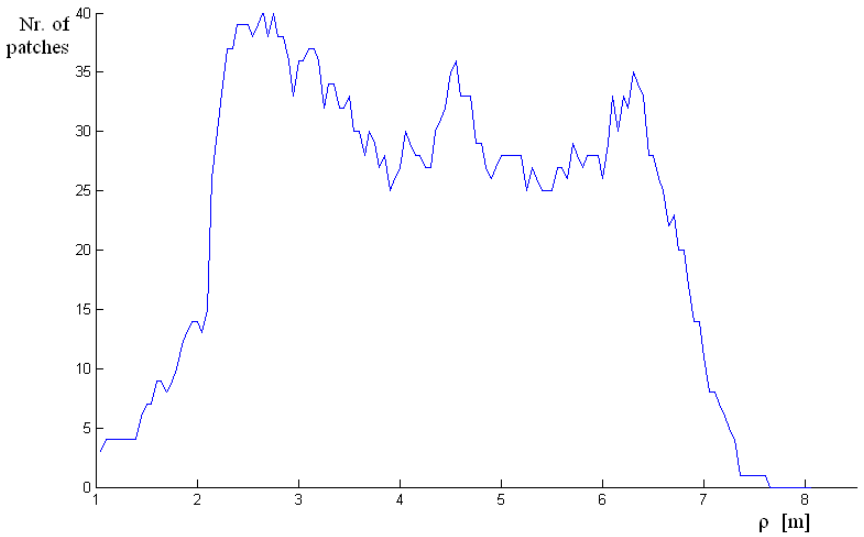

Fig. 8: Number of patches covering the range intervals of size 5 cm in the three scans used. At maximum almost 40 patches cover the intervals between 2.5 m and 3 m. The entire data set consists of 73 individual patches. Because of the high resolution of the scans most intervals contain about 300 measured laser points and all these are used in the adjustment.

In Fig. 7 the data of two scan positions before and after the range correction is shown. The uncorrected datasets clearly show the effect of short-periodic errors (cf. Figs. 7.a and 7.b), whereas for the corrected datasets these errors are significantly reduced (cf. Figs. 7.d and 7.e). These figures visualize the vertical distances of the uncorrected and corrected laser points from the adjusted patches. The spatial distribution of the errors before and after the correction are similar; i.e. at locations where the typical distance of points from the adjusting patch is positive before the correction, it is also positive after the correction. This is the consequence of the small but existing non-planarity of the patches.

Figs. 7.c and 7.f show the difference between both scans before and after the range correction. This additionally demonstrates the improvement. In all the subfigures of Fig. 7 the spatial distribution of the errors shows a relatively sharp change along a line on the wall and the floor. This residual error is due to the still uncorrected angular errors.

As mentioned in Section 3.5 the number of unknown parameters in the correction function is high. Therefore it has to be checked that each range interval is covered with patches. For this purpose Fig. 8 shows the number of patches in each range interval used in the adjustment. It can be seen that most range intervalls are covered by at least 25 different patches. Nonetheless, large correlations were found between the parameters a_i by analysing the inverse of the matrix of the normal equation system (18).

In order to test the stability of the results each possible pair of the three scanner positions was selected for determining the correction function. The three resulting correction functions were very similar to the result shown in Fig. 4, which results from using all three scanner positions simultaneously.

6 Conclusions

We presented an on-the-job calibration method for removing short-periodic systematic range errors in terrestrial laser scanner data using a piecewise linear range correction function, whose parameters are determined

using all measured points which lie in planar patches visible in the scanned scene. This correction function samples the span of the ranges with short intervals. Consequently this function has the benefit of being very general; thus practically no assumptions on the error sources are required. Its formulation, however, requires many parameters. Thus enough planar patches, which are range-wise overlapping (within the span of ranges on site) are required. Objects fulfilling this condition are, e. g., rooms.

In the presented example, with ranges up to 7 m, short-periodic systematic range errors were found and eliminated from the dataset using the proposed method. The short-periodic errors found correspond to the shortest modulating wavelength (1.2 meter) of the FARO LS 880HE instrument. It should be emphasized, that these wavelengths were not introduced into the model, but obtained from the correction function using Fourier analysis. Compared to the method of estimating the parameters of harmonic functions, we did not assume constant amplitudes along the whole measurement range. The correction function obtained proved to be time-independent – at least during the time interval of the three scans used in the example.

The application of piecewise linear functions proved to be effective for on-the-job calibration of range measurements. In the presented example this is shown by the improvement of the data quality, which can be seen clearly by comparing Fig. 7.a, b with Fig. 7.d, e.

In the future, we will test the proposed method on more examples, especially ones with larger spans of ranges. Further we will apply it also for the on-the-job calibration of the angular measurements of terrestrial laser scanners. This will require the formulation of the adjustment in the Gauss-Helmert model, which then will also allow the simultaneous on-the-job calibration of angles and ranges. Besides using it in *practice* as correction tool, the proposed function may be also beneficial for *research*. There it could be used as tool for studying the error behavior of the measurements by analyzing its computed form, e. g., with Fourier transformation. This way new correction functions, optimized with respect to shape, e. g., harmonics and/or polynomial, and number of parameters could be derived easier.

Acknowledgements

We would like to thank the private management of Schönbrunn Palace and Steinmetzbetriebe Bamberger as members of the Christian Doppler-Laboratory for supporting our investigations. Furthermore, we thank the anonymous reviewers for their fruitful and encouraging comments, which helped a lot in preparing the final version of the document.

References

Amiri Parian, J. & Gruen, A., 2005: Integrated laser scanner and intensity image calibration and accuracy assessment. – International Archives of the Photogrammetry, Remote Sensing and Spatial Information Sciences **36** (3/W19): 18–23.

Bae, K.H., Belton, D. & Lichti, D.D., 2005: A framework for position uncertainty of unorganized three-dimensional point clouds from near-monostatic laser scanners using covariance analysis. – International Archives of the Photogrammetry, Remote Sensing and Spatial Information Sciences **36** (3/W19): 7–12.

Bae, K.H. & Lichti, D.D., 2007: On-site self-calibration using planar features for terrestrial laser scanners. – International Archives of the Photogrammetry, Remote Sensing and Spatial Information Sciences **36** (3/W52): 14–19.

Dorninger, P. & Nothegger, C., 2007: 3D Segmentation of unstructured point clouds for building modeling. – International Archives of the Photogrammetry, Remote Sensing and Spatial Information Sciences **36** (3/W49A): 191–196.

Dorninger P., Nothegger, C., Pfeifer, N. & Molnar, G., 2008: On-the-job detection and correction of systematic cyclic distance measurement errors of terrestrial laser scanners. – Journal of Applied Geodesy **2** (4).

Gielsdorf, F., Rietdorf, A. & Gruendig, L., 2004: A Concept for the calibration of terrestrial laser scanners. – FIG Working Week 2004, Athens, Greece, May 22–27, on CD-ROM.

Ingensand, H., Ryf, A. & Schulz, T., 2003: Performances and Experiences in Terrestrial Laserscanning. – Optical 3-D Measurement Techniques VI, Zurich, Switzerland: 236–243.

KERSTEN, TH., MECHELKE, K., LINDSTAEDT, M. & STERNBERG, H., 2008: Geometric Accuracy Investigations of Latest Terrestrial Laser Scanning Systems. – FIG Working Week 2008, Integrating Generations, Stockholm, Sweden, June 14–19.

KRAUS, K., 1997: Photogrammetry, Volume 2, Advanced Methods and Applications. – Ferd. Dümmler Verlag, Bonn, Germany.

LICHTI, D.D., 2007: Error modeling, calibration and analysis of an AM-CW terrestrial laser scanner system. – ISPRS Journal of Photogrammetry and Remote Sensing **61** (5): 307–324.

MIKHAIL, E.M., 1976: Observations and Least Squares. – IEP – a Dun-Donnelley Publisher, New York, USA, 497 p.

NOTHEGGER, C. & DORNINGER, P., 2009: 3D Filtering of High-Resolution Terrestrial Laser Scanner Point Clouds for Cultural Heritage Documentation. – Photogrammetrie – Fernerkundung – Geoinformation **2009** (1): 607–617.

RÜEGER, J.M., 1990: Electronic distance measurement. – Springer-Verlag, Berlin, Germany.

SCHNEIDER, D. & MAAS, H.-G., 2007: Integrated bundle adjustment with variance component estimation – fusion of terrestrial laser scanner data, panoramic and central perspective image data. – International Archives of the Photogrammetry, Remote Sensing and Spatial Information Sciences **36** (3/W52): 18–23.

Addresses of the Authors:

PhD. GÁBOR MOLNÁR, Dr. PETER DORNINGER, Dipl.-Ing. CLEMENS NOTHEGGER, CHRISTIAN DOPPLER Laboratory for "Spatial Data from Laser Scanning and Remote Sensing" at the Institute of Photogrammetry and Remote Sensing, Vienna University of Technology, A-1040 Vienna, Gußhausstraße 27-29. Tel.: +43-1-58801-12250, Fax: +43-1-58801-12299, e-mail: {gmo, pdo, cn}@ipf.tuwien.ac.at

Prof. Dr. NORBERT PFEIFER, Dr. CAMILLO RESSL, Institute of Photogrammetry and Remote Sensing, Vienna University of Technology, A-1040 Vienna, Gußhausstraße 27–29., e-mail: {np, car}@ipf.tuwien.ac.at

Manuskript eingereicht: Juni 2008
Angenommen: November 2008